IEEE Access
Multidisciplinary | Rapid Review | Open Access Journal

Received September 27, 2020, accepted October 11, 2020, date of publication November 6, 2020, date of current version November 19, 2020.

Digital Object Identifier 10.1109/ACCESS.2020.3035504

Energy Arbitrage Optimization With Battery Storage: 3D-MILP for Electro-Thermal Performance and Semi-Empirical Aging Models

VOLKAN KUMTEPELI[1], HOLGER C. HESSE[2], MICHAEL SCHIMPE[2], ANSHUMAN TRIPATHI[3], YOUYI WANG[4], (Senior Member, IEEE), AND ANDREAS JOSSEN[2]

[1]Interdisciplinary Graduate School, Energy Research Institute @ NTU, Nanyang Technological University, Singapore 637141
[2]Department of Electrical and Computer Engineering, Technical University of Munich (TUM), 80333 Munich, Germany
[3]Energy Research Institute @ NTU, Nanyang Technological University, Singapore 637141
[4]School of Electrical & Electronic Engineering, Nanyang Technological University, Singapore 637141

Corresponding author: Holger C. Hesse (holger.hesse@tum.de)

This work was supported by the Technical University of Munich (TUM) in the framework of the Open Access Publishing Program and the Energy Research Institute, Nanyang Technological University (ERI@N), Singapore, within the joint project agreement International Center for Energy Research (ICER).

ABSTRACT Dispatch of battery storage systems for stationary grid applications is a topic of increasing interest: due to the volatility of power system's energy supply relying on variable renewable energy sources, one foresees a rising demand and market potential for both short- and long-term fluctuation smoothing via energy storage. While the potential revenue attainable via arbitrage trading may yet surpass the steadily declining cost of lithium-ion battery storage systems, profitability will be constrained directly by the limited lifetime of the battery system and lowered by dissipation losses of both battery and power electronic components. In this study, we present a novel three-dimensional mixed-integer program formulation allowing to model power, state of charge (SOC), and temperature dependence of battery dynamics simultaneously in a three dimensional space leveraging binary counting and union-jack triangulation. The inclusion of a state-of-the-art electro-thermal degradation model with its dependence on most influential physical parameters to the arbitrage revenue optimization allows to extend the battery lifetime by 2.2 years (or 40%) over a base scenario. By doing a profitability estimation over the battery's lifetime and using 2018 historical intraday market trading prices, we have shown that profitability of the system increases by 11.14% via introducing SOC awareness and another significant 12.64% via introducing thermal sensitivity, resulting in a total 25.19% increase over the base case optimization formulation. Lastly, through the open source publication of the optimization routines described herein, an adaption and development of the code to individual needs is facilitated.

INDEX TERMS Temperature effects on battery aging, energy arbitrage markets, optimization, mixed-integer linear-programming in three dimensions, piece-wise affine approximation, utility-scale storage, open-source code, lithium-ion.

ACRONYMS

AC	alternating current
BESS	battery energy storage system
BMS	battery management system
DOD	depth of discharge
EOL	end of life
FEC	full equivalent cycle
IDM	intraday market
LFP	lithium-iron-phosphate
MILP	mixed integer linear program(ming)
MPC	model predictive control
PWA	piecewise affine
RES	renewable energy source
SOC	state of charge
SOH	state of health
SOS2	special ordered set 2
TMS	thermal management system

The associate editor coordinating the review of this manuscript and approving it for publication was Sanjeevikumar Padmanaban.

I. INTRODUCTION

Day by day, power generation of volatile renewable energy sources (RESs) like wind and solar power generation is becoming more important, with an increasing demand for a sustainable grid infrastructure. However, their intermittent nature causes an imbalance in generation and consumption that is difficult to compensate for, via traditional generation units. Although deploying additional generation and extended grid infrastructure may be a remedy in some cases, a market-oriented approach will involve the consumers' awareness to curb their power demand by incentivizing them via dynamic electricity pricing. Consequently, in those countries allowing varying electricity prices and liberalized energy markets, the opportunity of energy arbitrage trading via deployment and operation of energy storage systems emerges [1]. To monetize price fluctuations, batteries stand out as a promising candidate among other energy storage technologies, due to their fast response, high efficiency, and declining investment costs. However, despite their rapidly declining prices and improving capabilities, battery energy storage systems (BESSs) are yet to be economically feasible in most applications [2]. Thus, their optimized operation plays a major role in reducing their cost.

The importance of battery degradation and power electronic losses is already emphasized in the literature [3]–[6]. However, there still is a gap between advances in grid connected battery system models and the respective optimization procedures. In this study, we focus on including detailed battery costs in the optimization algorithm and build a so-called an aging-aware battery management system (BMS) that helps to assess and optimize economic profitability more accurately. Although different battery dispatch optimization formulations are used in the literature [7]–[9], the effects of battery temperature are typically not fully included. However, as discussed in [10], temperature plays an important role in battery characteristics such as cell resistance, entropy, hysteresis voltage and self-discharge. It is also known that battery aging is massively affected by the cell temperature [11], [12]. Therefore, a suitable temperature model is essential to capture battery degradation accurately. For this reason, we propose an optimization procedure considering a detailed BESS model covering both thermal dynamics as well as state of charge (SOC) effects.

In this study, among different type of lithium-ion batteries, we confine our parametrization to a state-of-the-art lithium-iron-phosphate (LFP) cathode type since its cost/aging characteristics are balanced [13] and their suitability for heavy cycling grid applications has been proven [14]. For performance estimations, we rely on an equivalent circuit model allowing us to model the battery electrical states accurately [10], [15], as in the open-source BESS simulation tool, *SimSES* [16]. For aging estimation, we use the holistic model given in [12], which is parameterized for the LFP chemistry.

II. RELATED WORK

Power grids with increasing shares of distributed and variable RESs do not only demand for new measures of stability but do also favor volatility of energy trading markets [17], [18]. While battery storage is technically suitable to serve a number of different applications including grid stabilization and energy arbitrage market participation, the challenges in operational control may differ vastly. As has been underlined in a detailed review by Weitzel *et al.* [19], usage-related and sophisticated storage system and market models are required to estimate the dispatch behavior and economic revenue potential of a storage system. Such models are typically highly non-linear and require advanced heuristic, meta-heuristic or decomposition-based modeling techniques. For profit-optimized system control with consideration of variable costs, Schimpe *et al.* introduced the metric *marginal costs* which calculated the costs for energy losses and battery degradation occurring under operation of battery systems [20]. In the subsequent work by Hesse *et al.*, the cost metric was implemented in battery system control through mixed integer linear programming (MILP) formulation [7]. The implementation showed MILP as a stable real-time control technique for battery systems with variable price signals. Therefore, MILP appears to be a suitable approach for the problem formulated within the exact solution approaches, for a more detailed discussion on the individual advantages and shortcomings, the reader is referred to the original paper by Hesse *et al.* [7].

In other studies, Reniers *et al.* compared different modeling approaches for optimized control of battery systems [21]. Fortenbacher *et al.* considered optimized operation, however without covering thermal aspects during operation [2]. Arcos *et al.* used MILP to evaluate system control however used constant efficiency values to model energy losses [1].

Regarding the calculation of costs related to the battery aging, modeling of battery degradation was extensively covered by Naumann *et al.* for calendar and cycle aging of LFP-C cells [14], [22]. Schimpe *et al.* described a model for LFP-C cells with a focus on temperature dependency of cycle aging [12], [23], [24], which is used in this study.

Yilmaz *et al.* [25] used model predictive control and MILP in combination to tackle the battery dispatch problem in a microgrid. Yet, they have only considered cycling-induced aging via a generic method considering remaining number of cycles. Metz *et al.* in [26] explored the arbitrage opportunity for 15- and 60-minutes intraday markets in Germany. They restricted BESS response to small price variations by involving an aging related term in the cost function. However, constant aging coefficients were used to calculate calendar and cycle aging and only the dominant aging factor was considered. The study by Jafari *et al.* in [27] used a battery degradation model for NMC type batteries, built upon the study by Sakti *et al.* in [28]. The effect of representing battery degradation in off-shore wind energy storage systems was investigated. Although they mention the effect of temperature

and SOC on battery degradation, they do not include temperature effects in the optimization. Moreover, they use a depth of discharge (DOD) based cycle aging representation, whereas we propose a holistic approach with a focus on representation of temperature effects.

Lastly, modeling high-dimensional MILP problems still constitutes a part of the literature that is not deeply explored. The most prominent work is the systematic approach proposed by Misener *et al.* [29]. However, their study does not take the state-of-the-art logarithmic formulations in [30], [31] into account.

A. CONTRIBUTION STATEMENT

In this study, we create an optimization procedure that is able to take varying SOC and temperature effects into account via an efficient formulation for the constructed three-dimensional MILP problem by extending two-dimensional union-jack triangulation and logarithmic formulations demonstrated in [30], [31] into three-dimensional space. Specifically:

- A novel mixed-integer linear program formulation to encapsulate the detailed aging model is presented.
- To the best of our knowledge, thermal aspects and their impact on battery aging are included in an optimization for the energy arbitrage context for the first time.
- By detailed modeling of battery dynamics and power electronics as well as thermal dynamics, impact of different operational strategies on SOH evolution and energy losses is assessed and profitability expectation over the battery lifetime is provided.
- The paper is accompanied by the open-source code to enable practitioners to adapt the proposed methodology into their system.[1]

III. METHODOLOGY

With the overall system schematic given in Fig. 1, this section provides the methodology followed for BESS modeling and optimization problem formulation.

A. BATTERY MODELING

BESSs consist of many individual electrochemical units called *cells* that are connected in series and/or parallel fashion [32]. For simplicity, the modeling approach used in this study is based on single cell variables where these variables are scaled up to the system level linearly thanks to the negligible inhomogeneities between battery packs, given the battery cell chosen in this work [33]. In Fig. 1, the basic equivalent model of a cell is given with an illustration of the BESS schematic. Here, U_{OCV} and U_{T} represent the open-circuit voltage and terminal voltage of the cell respectively, and the difference between these two voltages is denoted by ΔU. Then, ΔU can be expanded as in (1) [10].

$$\Delta U = U_{\mathrm{T}} - U_{\mathrm{OCV}} = I_{\mathrm{cell}} \cdot R_{\mathrm{i}}(SOC, T) + \mathrm{sgn}(I_{\mathrm{cell}}) \cdot U_{\mathrm{hys}}(SOC) \quad (1)$$

[1]The link for the open-source code for this study can be found at www.SimSES.org along with other useful toolboxes.

where I_{cell}, R_{i}, U_{hys} are the cell current, internal resistance and hysteresis voltage respectively. $\mathrm{sgn}(I_{\mathrm{cell}})$ is the sign function which outputs -1 for negative values of I_{cell} (discharging) and $+1$ for positive values (charging). The cell power dissipation is calculated by (2) [10], [34].

$$\dot{Q}_{\mathrm{cell}} = I_{\mathrm{cell}} \left(\Delta U + T \cdot \frac{dU_{\mathrm{OCV}}}{dT} \bigg|_{T=T_{\mathrm{ref}}}(SOC) \right) \quad (2)$$

where dU_{OCV}/dT is the entropy in V/K, and T is the temperature in Kelvin. Numerical values for entropy, hysteresis voltage, and internal resistances are obtained by experimental measurements and can be found in [10]. Matching the specific battery cell characteristics, the SOC is chosen as (3), self-discharge is neglected, and the coulombic efficiency is set to 1 [35].

$$SOC(t) \approx \int_0^t \frac{I_{\mathrm{cell}}(\tau)}{C_{\mathrm{nom}} \cdot SOH(\tau)} d\tau \quad (3)$$

Here, C_{nom} is the nominal capacity of the cell in Ah and C_{r} is the C-rate of the battery [7].

$$FEC(t) = 0.5 \times \int_0^t \left| \frac{d}{d\tau} SOC(\tau) \right| d\tau \quad (4)$$

$$\approx 0.5 \times \int_0^t \frac{|P_{\mathrm{b}}(\tau)|}{E_{\mathrm{nom}}} d\tau \approx 0.5 \times \int_0^t C_{\mathrm{r}}(\tau) d\tau \quad (5)$$

Q_{Ah} is charge throughput given by (6).

$$Q_{\mathrm{Ah}}(t) = \int_0^t |I_{\mathrm{cell}}(\tau)| d\tau \quad (6)$$

For more information on battery modeling, the reader is referred to [32], [36].

B. OPTIMIZATION PROBLEM FORMULATION

In this section, we present the novel three-dimensional MILP based optimization method. Equations are constructed in a discrete manner and model with a prediction horizon of N_{h} is built. Unless otherwise specified, n denotes time step and $\forall n \in \mathbb{I}_{[1:N_{\mathrm{h}}]}$. Here, $n = 0$ is reserved for initial conditions of the system states which have $N_{\mathrm{h}} + 1$ elements with indices ranging from 0 to N_{h}. Variables with $+$ and $-$ superscripts denote charging and discharging respectively (e.g., I^{+}_{cell} is charging current and is equal to I_{cell} when charging and zero when discharging).

First, the model is defined via battery system power (at the battery pack terminals) P_{b}. Then, the battery power is linked with the AC-side power P_{AC} via (7)–(8).

$$P_{\mathrm{AC}}(n) = P_{\mathrm{b}}(n) + L_{\mathrm{AC}}(n) \quad (7)$$

$$-P^{\max}_{\mathrm{AC}} \leq P_{\mathrm{AC}}(n) \leq P^{\max}_{\mathrm{AC}} \quad (8)$$

where P_{AC} and L_{AC} are AC-side power and inverter losses, respectively. The AC-side power P_{AC} is limited by the maximum power of the inverter $P^{\max}_{\mathrm{AC}}$ and L_{AC} is given in Fig. 4 with its approximation is explained in Section III-E. AC-side power is distributed to all inverters with their respective battery racks evenly.

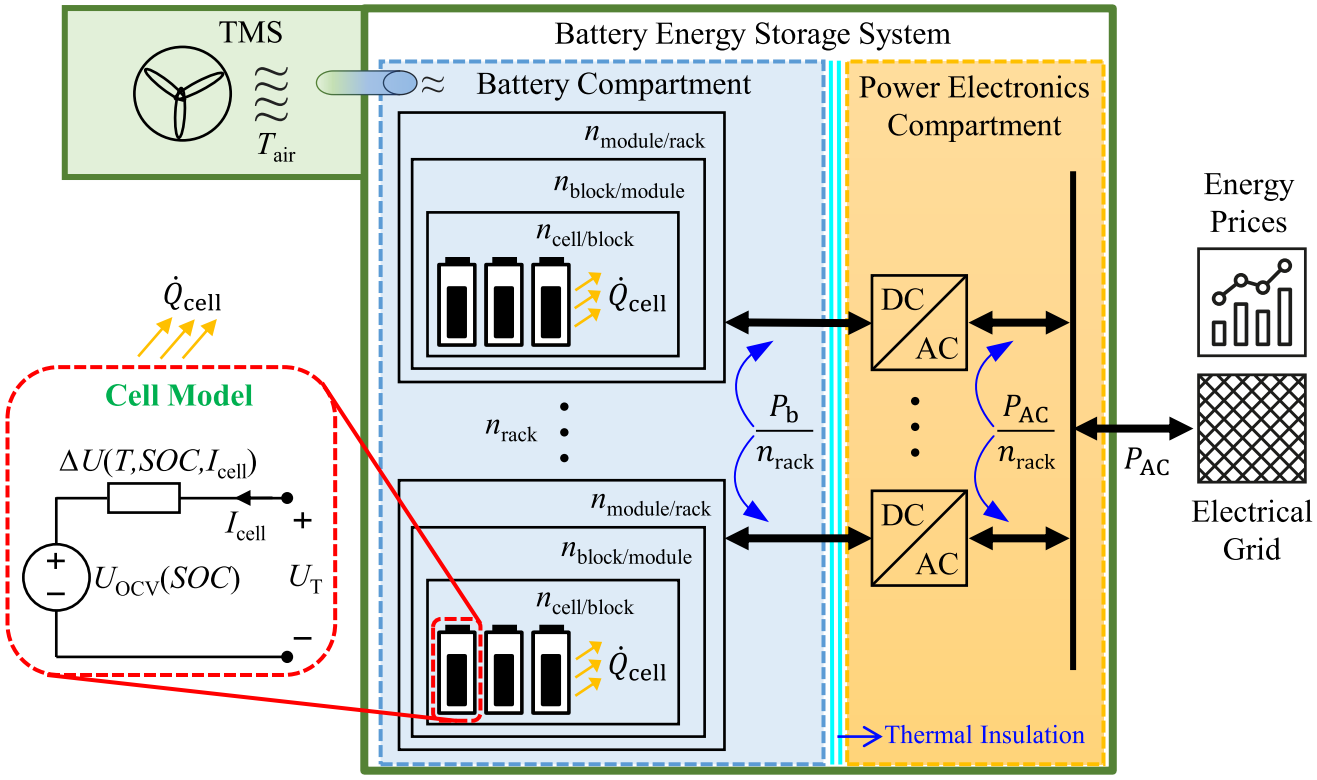

FIGURE 1. Schematic of a containerized utility-scale battery energy storage system consisting of multiple battery cells and AC/DC inverters for grid connection. Fan output air temperature is constant at $T_{air} = 18°$ C.

After denoting the system-scale variables, cell variables are given in following equations.

$$P_{cell}(n) = \frac{P_b(n)}{n_{cell/block} \cdot n_{block/module} \cdot n_{module/rack} \cdot n_{rack}} \quad (9)$$

where P_{cell} is the cell power and $n_{cell/block}$, $n_{block/module}$, $n_{module/rack}$, n_{rack} denote the number of cells per block, blocks per module, modules per rack and racks in the system respectively. Then, the energy stored in the battery is given in (10)–(13) [13].

$$C_{bat}(0) = 0 \quad (10)$$

$$C_{bat}(n) = C_{bat}(n-1) + I_{cell}(n)\Delta t \quad (11)$$

$$0 \leq C_{bat}(n) \leq C_{max}(n) \quad (12)$$

$$C_{max}(n) = SOH(t) \cdot C_{nom} \cdot (SOC_{max} - SOC_{min}) \quad (13)$$

Here, $C_{bat} \in \mathbb{R}^{(N_h+1)}$ denotes usable battery capacity that is constrained by a diminishing upper limit C_{max}. This representation is leveraged instead of SOC representation in [13] to make it easier to capture capacity loss effects as in [37]. Then the SOC can be retrieved by (14).

$$SOC(n) = SOC_{min} + C_{bat}(n)/(C_{nom} \cdot SOH(t)) \quad (14)$$

Lastly, C-rate is limited using (15) where $C^{+}_{r\text{-}max}$, $C^{-}_{r\text{-}max}$ denote charging and discharging C-rate limits respectively.

$$-C^{-}_{r\text{-}max} \leq \frac{I_{cell}(n)}{C_{nom} \cdot SOH(t)} \leq C^{+}_{r\text{-}max} \quad (15)$$

Here, I_{cell} is found by approximation as further described in Section III-F.

C. BATTERY AGING MODELING

The capacity of LFP batteries fades mainly due to the mechanisms such as lithium plating and growth of a solid electrolyte interphase layer [13]. A comprehensive discussion on the physical processes and definitions of aging factors can be found in [12] which also provides experimentally confirmed values for the fitted parameters. As mentioned, a holistic approach including calendar and cycle aging simultaneously is preferred for aging modeling. Considering the complete aging equation first presented in [12]:

$$\begin{aligned} Q_{loss}(t) = {} & k_{cal}(T, SOC)\sqrt{t} + k_{cyc,high\ T}(T)\sqrt{Q_{Ah}(t)} \\ & + k_{cyc,low\ T}(T, I^{+}_{cell})\sqrt{Q^{+}_{Ah}(t)} \\ & + k_{cyc,low\ T,\ high\ SOC}(T, I^{+}_{cell})Q^{+}_{Ah}(t) \end{aligned} \quad (16)$$

where k_{cal}, $k_{cyc,high\ T}$, $k_{cyc,low\ T}$ and $k_{cyc,low\ T,\ high\ SOC}$ are different aging factors that correspond to calendar aging and cycle aging at high temperature, low temperature and both low temperature and high SOC respectively.

After giving (16), it must be said that it is a cumulative function designed to work with constant factors; hence, it cannot be used directly [12]. Therefore, it should be converted to a rate-based equation as indicated by Thomas *et al.* [38], [39]. To avoid burden of refitting for obtaining rate-based

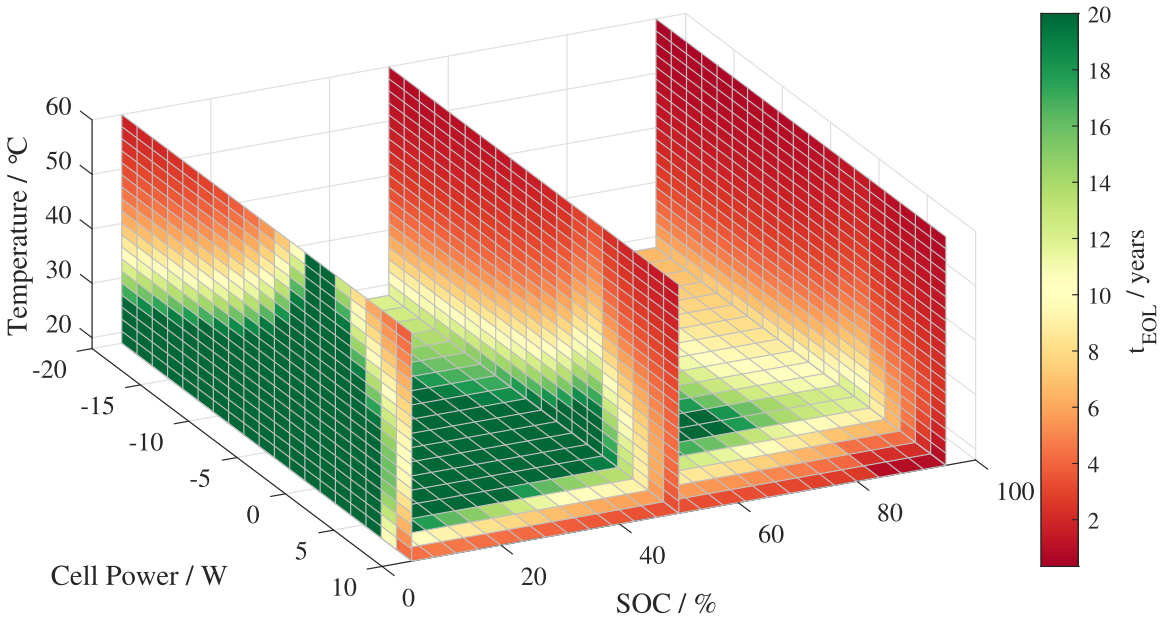

FIGURE 2. Lifetime expectation (t_{EOL}, solution of (17) for end-of-life conditions) considering both calendar and cycle aging for different configurations of cell power, SOC and cell temperature. Values beyond 20 years are not shown in the figure.

equations, we follow a similar yet easier approach. To do so, we modify (16) slightly. Considering that (16) is used with constant operating conditions, (6) can be approximated as $Q_{\text{Ah}}(t) \approx |I_{\text{cell}}| \cdot t$ (and $Q^{+}_{\text{Ah}}(t) \approx I^{+}_{\text{cell}} \cdot t$). Therefore, (16) becomes

$$\begin{aligned} Q_{\text{loss}}(t) &\approx k_{\text{cal}}(T, SOC)\sqrt{t} + k_{\text{cyc,high T}}(T)\sqrt{|I_{\text{cell}}|}\sqrt{t} \\ &\quad + k_{\text{cyc,low T}}(T, I^{+}_{\text{cell}})\sqrt{I^{+}_{\text{cell}}}\sqrt{t} \\ &\quad + k_{\text{cyc,low T, high SOC}}(T, I^{+}_{\text{cell}}) \cdot I^{+}_{\text{cell}} \cdot t \\ &= \Big(k_{\text{cal}}(T, SOC) + k_{\text{cyc,high T}}(T)\sqrt{|I_{\text{cell}}|} \\ &\quad + k_{\text{cyc,low T}}(T, I^{+}_{\text{cell}})\sqrt{I^{+}_{\text{cell}}}\Big) \cdot \sqrt{t} \\ &\quad + \big(k_{\text{cyc,low T, high SOC}}(T, I^{+}_{\text{cell}}) \cdot I^{+}_{\text{cell}}\big) \cdot t \end{aligned} \tag{17}$$

In terms of $\sqrt{t}$, $t \geq 0$, (17) can be solved as a quadratic equation. For a particular configuration of $(T, SOC, I_{\text{cell}}, Q_{\text{loss}})$, the equation can be solved for t. By substituting Q_{loss} with its maximum value at the end of life $k_{\text{EOL}} = 80\%$ [13], we can derive a maximum dwell time under constant conditions until reaching the end of life t_{EOL}. An illustration of t_{EOL} for some configurations is given in Fig. 2. As such, the cost for a particular configuration can be estimated by (18).

$$J_{\text{aging}}(T, SOC, I_{\text{cell}}) = \frac{c_{\text{bat}} \cdot E_{\text{nom}}}{t_{\text{EOL}}(T, SOC, I_{\text{cell}})} \Delta t \tag{18}$$

where c_{bat} is the battery cost per kWh and Δt is the time spend on a particular configuration. Lastly the objective function may be given as:

$$J = \sum_{n=1}^{N_{\text{h}}} \big(P_{\text{AC}}(n) c_{\text{en}}(n) + J_{\text{aging}}(n)\big) \tag{19}$$

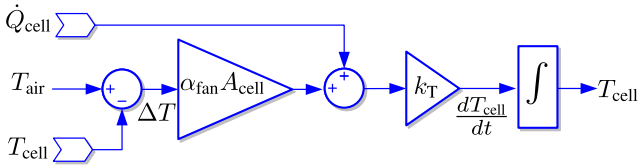

FIGURE 3. Block diagram of the BESS thermal dynamics.

$$J_{\text{aging}}(n) = J_{\text{aging}}(T_{\text{avg}}(n), SOC_{\text{avg}}(n), I_{\text{cell}}(n)) \tag{20}$$

where $c_{\text{en}}(n)$ is the price of energy and cost of aging $J_{\text{aging}}(n)$ will be approximated in Section III-F.

D. THERMAL MODELING

As discussed in [10], [40], temperature plays an important role in battery characteristics and battery health. Particularly calendar aging is massively effected by the cell temperature [12]. Therefore, a thermal model is essential to capture calendar aging accurately. Since large-scale stationary battery systems are kept in containers with an active cooling system, actual battery thermal characteristics may differ significantly. Therefore, it is also important to take the BESS container conditions into account to model the behavior of such a system at all times of the system usage at the location of battery cell. By assuming homogeneity between cells, constant input air flow temperature, and that the fan runs constantly at its nominal speed, thermal dynamics can be simplified resulting in a 0-degree lumped temperature dynamics model in Fig. 3 [41], [42].

In Fig. 3, $\dot{Q}_{\text{cell}}$, T_{air}, T_{cell} denote power dissipation on cell, temperature of the air blown by the fan, and cell temperature. A_{cell} is the battery area taken as $6.4 \cdot 10^{-3}$ m^2 and α_{fan} is

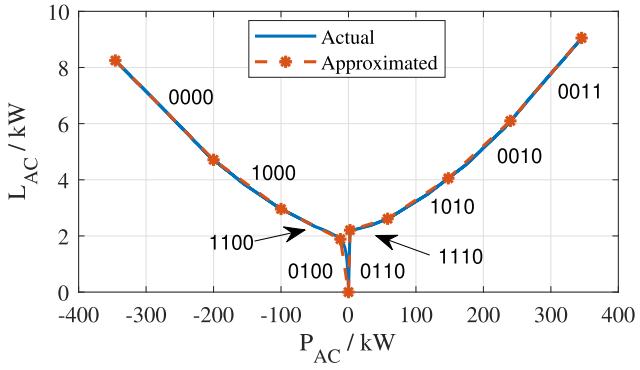

FIGURE 4. Power electronic equipment loss and its PWA approximation versus AC output power. Numbers denote binary sequences for the each line segment.

a coefficient related to fan speed; however, at nominal speed, $\alpha_{\text{fan}} = 3$ W/(m^2·K) [10]. Lastly, k_{T} is given by $k_{\text{T}} = 1/(m_{\text{cell}} \cdot C_{\text{p}})$ where m_{cell} is the mass of cell taken as 85 grams and C_{p} is the cell specific heat taken as 838 J/(kg·K). T_{air} is assumed to be constant at 18 °C. The definition of $\dot{Q}_{\text{cell}}$ is given by (2). $\dot{Q}_{\text{cell}}$, $\dot{T}$ are nonlinear functions to be approximated in Section III-F. Hence, thermal model reduces to (21) with the initial condition $T(0) = 25$ °C at the beginning of the simulation and soft limits in (22).

$$T(n) = T(n-1) + \Delta t \cdot \dot{T}(n) \tag{21}$$

$$T_{\min} \leq T(n) \leq T_{\max} \tag{22}$$

E. APPROXIMATION OF POWER ELECTRONICS EFFICIENCY

It is important to include variable power electronics efficiency for accurate prediction of the expected profit [7]. Therefore, in this subsection, we present the MILP formulation for estimating inverter losses L_{AC} using piecewise affine (PWA) approximation.

First, considering the desired accuracy, necessary data points for linear approximation is determined. The loss function $L_{\text{AC}}(P_{\text{AC}})$ and its approximation based on the selected vertices are given in Fig. 4 where $P_{\text{AC}} \geq 0$ indicates charging. This loss curve is obtained by by multiplying the curve in [7], due to having 8 identical racks with 8 inverters [10], [43].

As shown in Fig. 4, the domain of P_{AC} is divided into $N_{\text{P\_AC}} = 9$ segments resulting in a set of vertices $\nu_{\text{P\_AC}} \in \mathbb{R}^{(N_{\text{AC}}+1)}$ where $\nu_{\text{P\_AC}}(1) = -P_{\text{AC}}^{\max}$ and $\nu_{\text{P\_AC}}(N_{\text{P\_AC}} + 1) = P_{\text{AC}}^{\max}$. To linearly interpolate points in between vertices, convex combination of two subsequent vertices is used. For this reason, a weight matrix $\lambda_{\text{AC}} \in \mathbb{R}^{N_{\text{AC}}+1} \times \mathbb{R}^{N_{\text{h}}}$ is defined. As such, the loss approximation is written as (23)–(26).

$$P_{\text{AC}}(n) = \sum_{i=1}^{N_{\text{AC}}+1} \nu_{\text{P\_AC}}(i)\lambda_{\text{AC}}(i,n) \tag{23}$$

$$L_{\text{AC}}(n) = \sum_{i=1}^{N_{\text{AC}}+1} f_{\text{AC}}(\nu_{\text{P\_AC}}(i))\lambda_{\text{AC}}(i,n) \tag{24}$$

$$0 \leq \lambda_{\text{AC}}(i,n) \leq 1 \quad \forall i \in \mathbb{I}_{[1:N_{\text{AC}}+1]} \tag{25}$$

$$1 = \sum_{i=1}^{N_{\text{AC}}+1} \lambda_{\text{AC}}(i,n) \tag{26}$$

Definitions of above-given equations are straightforward where the formulation challenge generally stems from the satisfaction of the constraint that requires only weights of the subsequent vertices to be active. This constraint is called special ordered set 2 (SOS2) constraint and generally recognized by the state of art solvers [44], [45]. Although one may simply define a SOS2 constraint, studies done by Huchette and Vielma show that there exist much better formulations especially for larger problems [31], [46], [47]. Indicated methods reduce the number of binary variables logarithmically by leveraging the binary counting as opposed to the unary counting [48]. Hence, the number of required binary variables reduce to $d_{\text{AC}} = \lceil \log_2(N_{\text{AC}}) \rceil$. However, these result in a more complicated relationship between binary variables and weights. A simple procedure to reveal this relationship is given in [49]. Another complexity within this binary counting arises due to the necessity of using a neighborhood-preserving counting method. Therefore, between adjacent line segments, there should be minimal change of bits or hamming distance should be 1 [50]. For this reason, a particular sequence known as the binary reflected gray code [46] is used. Using this recursive algorithm, a gray code matrix with d_{AC} bits (or columns) and $2^{d_{\text{AC}}}$ rows is created. Then its first N_{AC} rows are selected as the gray code matrix and matched with each PWA segment respectively, as shown in Fig. 4. After naming each segment with a known binary sequence, we form a binary decision variable matrix $s_{\text{AC}} \in \mathbb{R}^{d_{\text{AC}}} \times \mathbb{R}^{N_{\text{h}}}$ to enable or disable relevant weights to activate the appropriate PWA segment. Then an indicator function is realized such that $\text{ind}(\nu, k, z)$ outputs 1 if and only if for the vertex ν, all of the k^{th} bit of the gray codes of the segments that the vertex is connected equal to z [49]. For example, second vertex is connected to the first and second line segments. As seen in Fig. 4, first segment's gray code is "0000" and second segment's is "1000". Considering $\text{ind}(\nu_{\text{AC}}(2), k, 0)$ for $k = 2, 3, 4$ would be 1 since both gray codes' digits are 0 for $k = 2, 3, 4$. However, for $k = 1$ the function would output 0 since not all of the gray codes' k^{th} digit is 0. Then the SOS2 constraint can be represented as follows.

$$\sum_i \lambda_{\text{AC}}(i,n) \leq s_{\text{AC}}(k,n) \quad \forall n \in \mathbb{I}_{[1:N_{\text{h}}]}, \quad \forall k \in \mathbb{I}_{[1:d_{\text{AC}}]}, \quad i \in \{i \mid \text{ind}(\nu_{\text{AC}}(i), k, 1) = 1\} \tag{27}$$

$$\sum_i \lambda_{\text{AC}}(i,n) \leq 1 - s_{\text{AC}}(k,n) \quad \forall n \in \mathbb{I}_{[1:N_{\text{h}}]}, \ \forall k \in \mathbb{I}_{[1:d_{\text{AC}}]}, \quad i \in \{i \mid \text{ind}(\nu_{\text{AC}}(i), k, 0) = 1\} \tag{28}$$

F. APPROXIMATION OF OTHER NONLINEARITIES

After approximating the efficiency of the power electronic equipment, the remaining nonlinearites to be addressed stem from the battery system dynamics. We propose and design a holistic approach in order to reach all desired variables by

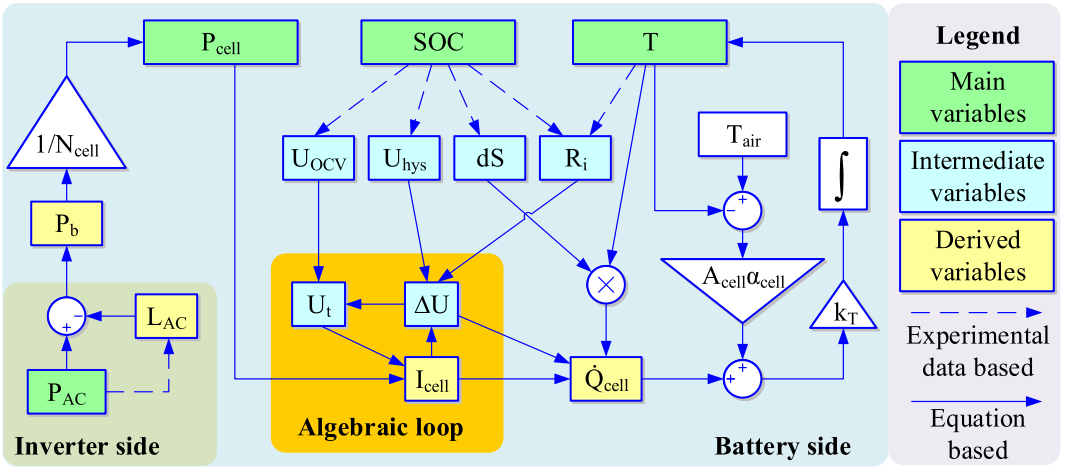

FIGURE 5. Relationship of the variables in the optimization problem formulation.

keeping the number of auxiliary variables at a reasonable level. Therefore, the three variables P_{cell}, SOC and T are selected as main variables for battery dynamics, all other variables are derived by relations as illustrated in Fig. 5.

We differentiate among four main variables (green blocks in Fig. 5) subdivided to three main variables for the battery and one (P_{AC}) for the inverter output power. Other variables are created being intermediate and derived variables (yellow and cyan blocks respectively). Dashed lines between blocks indicate that experimental data is used to find the variable, whereas a solid line between blocks denotes that the connection is established via an equation. It should be noted that, intermediate variables do not appear in the optimization and are used to calculate the derived variables only.

Since there are three main variables for battery dynamics, input space for approximation will be a 3-dimensional volume. Then this volume needs to be divided into smaller pieces which are used to interpolate the points in that region linearly. Therefore, each axis of the input space is divided into N_{Pcell}, N_{SOC} and N_{T} segments resulting in a $N_{\text{cuboid}} = N_{\text{Pcell}} \cdot N_{\text{SOC}} \cdot N_{\text{T}}$ pieces of rectangular prisms shown in Fig. 6a. However, linear approximation of the multivariate functions is not as straightforward as univariate functions. Although four points are enough to create a unique linear approximation, each cuboid contains eight different vertices. Achieving unique shapes with four vertices requires additional partitioning, such as R- or K-triangulation of each perpendicular side of the cuboid described in [29]. Although these type of triangulations seem to be simple enough, a more symmetrical triangulation can provide easiness of gray-code generation and pave the way for more advanced formulations. For this reason, union-jack triangulation shown in Fig. 6b, is preferred in this study as it is used in other studies such as Vielma *et al.* [31]. Detailed information and comparison also can be found in [30], [46], [51].

As being different from [29], the study by Vielma *et al.* [31] suggests the use of gray code encoding for each triangulation.

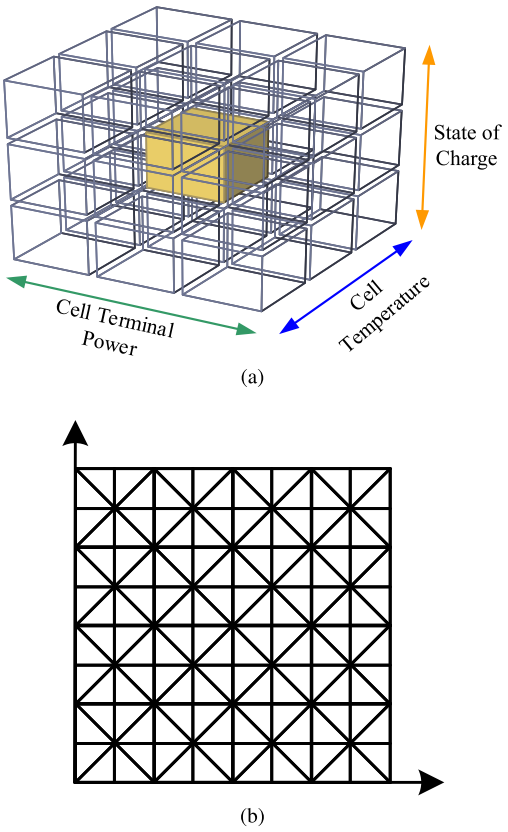

FIGURE 6. Approximation tessellation for (a) whole approximation space with rectangular prisms (the figure was adapted from [52]); (b) Union-jack triangulation of each side.

However, it only provides univariate and bivariate functions whereas our system requires modeling of a three-dimensional input space. Therefore, we provide gray-codes for one cube as shown in Fig. A1 in Appendix.

After having union-jack triangulation of one cube, the next step would be generating the whole cuboid by using one cube

as a building block. Since this structure is symmetric, its enumeration is straightforward as similar to a binary cube. The method in [50] for finding gray codes for 2-dimensional space can be easily extended to 3-dimensional space. The procedure used in this study to generate the gray codes is given by Algorithms A1 and A2.

After creating the gray code, four dimensional weight tensor $\lambda_{\text{cell}} \in \mathbb{R}^{(2N_{\text{Pcell}}+1)} \times \mathbb{R}^{(2N_{\text{SOC}}+1)} \times \mathbb{R}^{(2N_{\text{T}}+1)} \times \mathbb{R}^{N_{\text{h}}}$ for the vertices $\nu_{\text{cell}} = \nu_{\text{Pcell}} \times \nu_{\text{SOC}} \times \nu_{\text{T}}$ can be constrained as following, noting that using union-jack triangulation doubles number of segmentation. Then $\forall i \in \mathbb{I}_{[1:2N_{\text{Pcell}}+1]}$, $\forall j \in \mathbb{I}_{[1:2N_{\text{SOC}}+1]}$ and $\forall k \in \mathbb{I}_{[1:2N_{\text{T}}+1]}$, following equations are defined.

$$0 \leq \lambda_{\text{cell}}(i,j,k,n) \leq 1 \tag{29}$$

$$1 = \sum_{i=1}^{2N_{\text{Pcell}}+1} \sum_{j=1}^{2N_{\text{SOC}}+1} \sum_{k=1}^{2N_{\text{T}}+1} \lambda_{\text{cell}}(i,j,k,n) \tag{30}$$

with the following binary constraints [49]:

$$\sum_{i,j,k} \lambda_{\text{cell}}(i,j,k,n) \leq s_{\text{cell}}(u,i,j,k,n) \quad \forall u \in \mathbb{I}_{[1:d_{\text{cuboid}}]},$$
$$(i,j,k) \in \{i,j,k \mid \text{ind}(\nu_{\text{cell}}(i,j,k),u,1) = 1\} \tag{31}$$

$$\sum_{i,j,k} \lambda_{\text{cell}}(i,j,k,n) \leq 1 - s_{\text{cell}}(u,i,j,k,n) \quad \forall u \in \mathbb{I}_{[1:d_{\text{cuboid}}]},$$
$$(i,j,k) \in \{i,j,k \mid \text{ind}(\nu_{\text{cell}}(i,j,k),u,0) = 1\} \tag{32}$$

where s_{cell} is the tensor holding binary decision variables to activate the necessary vertices. Thanks to the holistic gray-code enumeration approach, above-given constraints are enough the select unique vertices, any other SOS2 constraints are not required as in [29], [53].

After defining all auxiliary constraints that activate the appropriate vertices in the three dimensional volume, relationship between these auxiliary and actual variables can be established.

$$P_{\text{cell}}(n) = \sum_{i=1}^{2N_{\text{Pcell}}+1} \sum_{j=1}^{2N_{\text{SOC}}+1} \sum_{k=1}^{2N_{\text{T}}+1} \nu_{\text{Pcell}}(i,j,k) \cdot \lambda_{\text{cell}}(i,j,k,n) \tag{33}$$

$$SOC_{\text{avg}}(n) = \sum_{i=1}^{2N_{\text{Pcell}}+1} \sum_{j=1}^{N_{\text{SOC}}+1} \sum_{k=1}^{2N_{\text{T}}+1} \nu_{\text{SOC}}(i,j,k) \cdot \lambda_{\text{cell}}(i,j,k,n) \tag{34}$$

$$T_{\text{avg}}(n) = \sum_{i=1}^{2N_{\text{Pcell}}+1} \sum_{j=1}^{2N_{\text{SOC}}+1} \sum_{k=1}^{2N_{\text{T}}+1} \nu_{\text{T}}(i,j,k) \cdot \lambda_{\text{cell}}(i,j,k,n) \tag{35}$$

where SOC_{avg} and T_{avg} are the average SOC and temperature in between time steps and defined as

$$SOC_{\text{avg}}(n) = (SOC(n-1) + SOC(n))/2 \tag{36}$$

$$T_{\text{avg}}(n) = (T(n-1) + T(n))/2 \tag{37}$$

The reason for using average values for SOC and T is that they change between beginning and end of the time step. Therefore, for each time step, their average values are considered with an assumption that they change linearly. Consequently, their average values determine the operating point for PWA approximation. Then other nonlinear variables can also be approximated using the weight matrix λ_{cell}. Approximation of the aging cost function J_{aging}, the heat dissipation $\dot{Q}_{\text{cell}}$, the temperature change $\dot{T}_{\text{cell}}$ and the current I_{cell} is straightforward with the help of vertices ν_{aging}, ν_{dQ} and ν_{dT}, ν_{I}, $\forall n \in \mathbb{I}_{[1:N_{\text{h}}]}$.

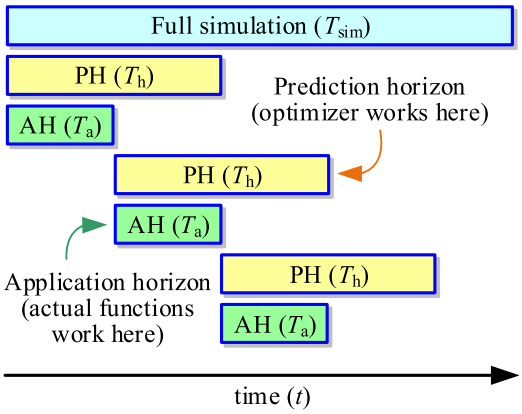

FIGURE 7. Illustration of the used rolling horizon scheme.

$$J_{\text{aging}}(n) = \sum_{i=1}^{2N_{\text{Pcell}}+1} \sum_{j=1}^{2N_{\text{SOC}}+1} \sum_{k=1}^{2N_{\text{T}}+1} \nu_{\text{aging}}(j,k)\lambda_{\text{cell}}(i,j,k,n) \tag{38}$$

$$\dot{Q}(n) = \sum_{i=1}^{2N_{\text{Pcell}}+1} \sum_{j=1}^{2N_{\text{SOC}}+1} \sum_{k=1}^{2N_{\text{T}}+1} \nu_{\text{dQ}}(i,j,k)\lambda_{\text{cell}}(i,j,k,n) \tag{39}$$

$$\dot{T}(n) = \sum_{i=1}^{2N_{\text{Pcell}}+1} \sum_{j=1}^{2N_{\text{SOC}}+1} \sum_{k=1}^{2N_{\text{T}}+1} \nu_{\text{dT}}(i,j,k)\lambda_{\text{cell}}(i,j,k,n) \tag{40}$$

$$I_{\text{cell}}(n) = \sum_{i=1}^{2N_{\text{Pcell}}+1} \sum_{j=1}^{2N_{\text{SOC}}+1} \sum_{k=1}^{2N_{\text{T}}+1} \nu_{\text{I}}(i,j,k)\lambda_{\text{cell}}(i,j,k,n) \tag{41}$$

In this study, to determine vertices optimally, the approach used in [7], [54]–[56] is adapted to handle 3 dimensional data: assuming that the system can be approximated by a gridded data (i.e., not randomly scattered in the three dimensional input space). Hence, only the data points lying at the axes were optimally selected with the help of MATLAB's *fmincon* solver and *griddedInterpolant* functions. Lastly, we define the constraint in (42) to make the simulation faster by removing some of the unnecessary branching.

$$P_{\text{b}}(n) \leq P_{\text{AC}}(n) \tag{42}$$

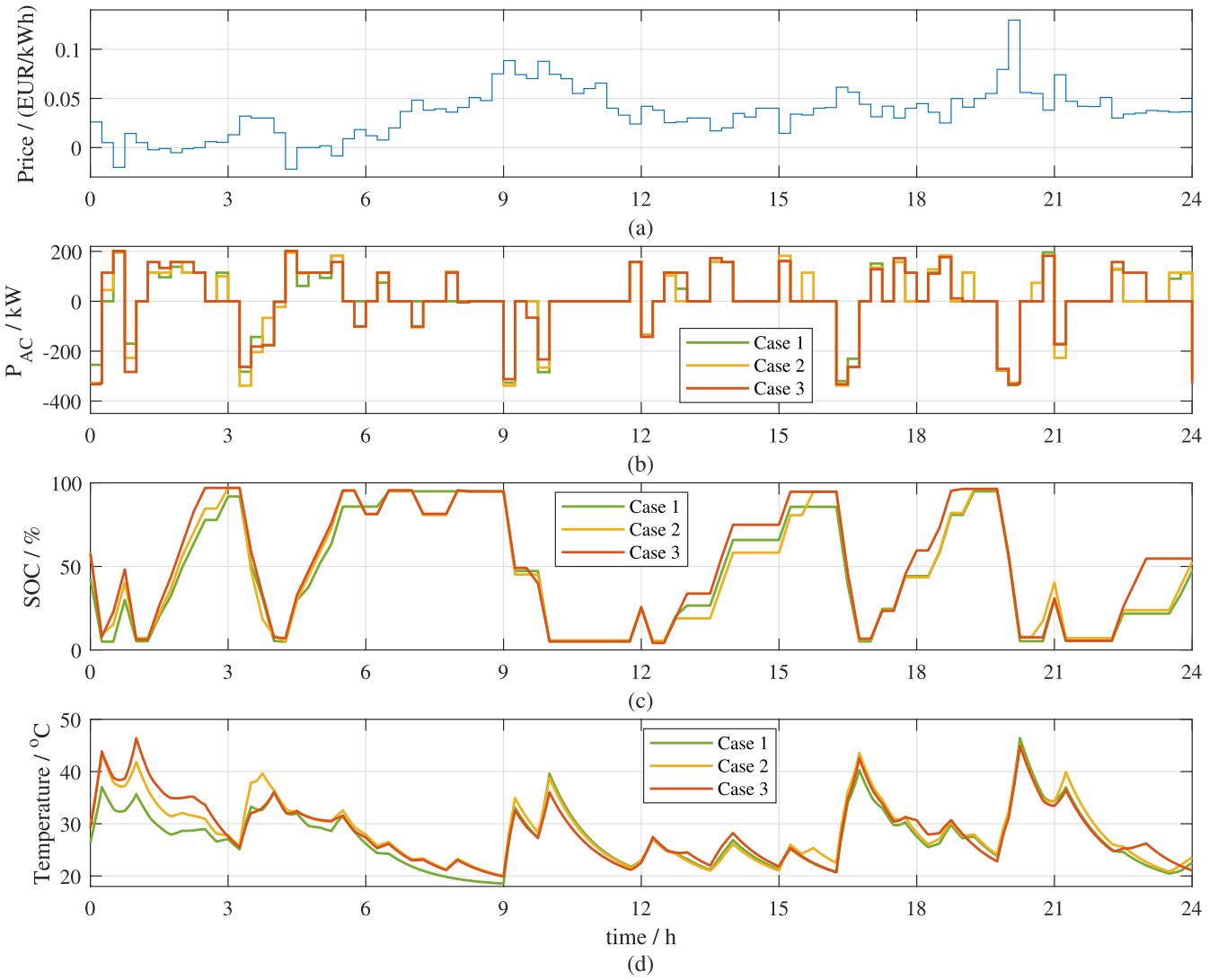

FIGURE 8. Time series plot of the day with the price variance closest to the mean price variance. Case 1: temperature and SOC aware 3D optimization, case 2: only SOC aware 2D optimization, case 3: 1D optimization with fixed SOC and temperature assumption.

IV. RESULTS AND DISCUSSION

With the given details of the proposed framework in this section, an illustrative case study is provided. To test the system, an energy arbitrage scenario as in [7] is used. However, instead of conducting a batch simulation, a rolling horizon algorithm is preferred to keep computation time at reasonable levels [57]. In this scheme, the optimization problem is solved with N_h time steps (i.e., $T_h/\Delta t$), then first N_a steps (i.e., $T_a/\Delta t$) are applied to the BESS. To apply the power reference, the system is simulated using original nonlinear equations with a smaller time step δt. With T_{sim}/T_a iterations, a desired simulation time of T_{sim} is achieved. This iteration scheme is illustrated in Fig. 7. It should also be noted that with the help of this receding horizon simulation strategy, it is possible to simplify the optimization problem further. For example, constraints in (13)–(15) are simplified by keeping the state of health (SOH) value in the optimization constant and updating it at the beginning of each optimization loop. With this system setup, numerical values regarding this case study can be found in Table A1 in Appendix.

To illustrate the effect of considering temperature and SOC dynamics in the optimization, we generated three case studies: case 1, where both effects are considered in the optimization; case 2, where only SOC effect is considered in the optimization; and, lastly, case 3, where both of the effects are neglected in the optimization.

To analyze the effect of including temperature dynamics in the optimization, case 1 is constructed according to equations given above (temperature and SOC aware modeling). However, in cases 2, 3 the temperature is assumed constant at $T_{constant} = 25$ °C by modifying (20) and (21) as in (43) and (44).

$$J_{aging}(n) = J_{aging}(T_{constant}, SOC_{avg}(n), I_{cell}(n)) \quad (43)$$

$$T(n) = T_{\text{constant}} \quad \forall n \in \mathbb{I}_{[0:N_h]} \tag{44}$$

On the other hand, when simulating the absence of SOC effect in case 3, it is not completely fixed in the optimization not to ignore the SOC limits completely. Instead, only (20) is changed to (45) to ignore SOC effect on the cost.

$$J_{\text{aging}}(n) = J_{\text{aging}}(T_{\text{constant}}, SOC_{\text{constant}}, I_{\text{cell}}(n)) \tag{45}$$

Using the above-given equations, proposed framework is implemented using YALMIP [58] and Gurobi [59]. Thanks to the proposed method combining several state-of-the-art approaches, it was possible to solve this highly-complex problem efficiently by increasing solution speed and reducing memory consumption due to having less binary variables. Hence, applying our method to the historical last values of the intraday market trading prices of 2018 [60], we obtain the following results.

First, in Fig. 8, we present time series results regarding the day with price variations closest to the mean price variations to have a rough idea about the overall optimization. In Fig. 8a, b, c, and d; price signal, AC-side power P_{AC}, SOC, and cell temperature T variables are given respectively. Considering the charging/discharging patterns and SOC levels, we may infer that case 1 prefers lower P_{AC} levels compared to case 2 which also prefers lower P_{AC} levels compared to case 3. As expected, SOC levels are lower in case 1 and 2 due to the SOC awareness of the optimizer and calendar aging being more pronounced when resting at a higher SOC. Moreover, in case 1 and 2, the optimizer also tries to postpone charging to keep the overall SOC lower. Due to the temperature effect on the cost, in case 1 the optimizer only dispatches the battery in cases of higher price fluctuations resulting in dissipative heating and additional aging impacts recognized by the optimizer, whereas in case 2 and 3 it already responds to smaller price changes being unaware of the dissipation loss side effects. Lastly, as seen in Fig. 8d, the optimizer with the temperature awareness (case 1) keeps the cell temperature lowest at a mean value of 28.96 °C.

After analyzing the time series plot in Fig. 8, we may see the long-term decisions of the optimizer decisions in Fig. 9 where the cumulative frequency plot of the AC-side power is given. Different than Fig. 8b, we can now clearly see in Fig. 9 that the optimizer tends to keep P_{AC} lower to reduce the overall cell temperature. On the other hand, in cases 2 and 3, P_{AC} pattern seems to be similar as expected since SOC does not directly depend on the power level but the energy throughput. Therefore, in these cases, there is not a strong driving reason for the optimizer to decide in favor of lower power levels.

Long-term effects of the proposed algorithm on temperature and SOC are given in the rain-cloud plots and histograms in Fig. 10. For illustration of rain clouds open-source libraries given in [61], [62] with color schemes in [63] are utilized. As settings, *ksdensity* function of MATLAB with a triangle kernel is preferred. By considering probability densities in Figs. 10a–c, we see that temperature distribution in case 1 is

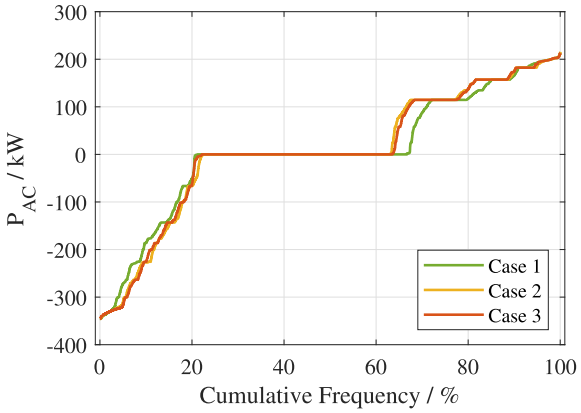

FIGURE 9. P_{AC} differences due to temperature and SOC inclusion. Case 1: temperature and SOC aware 3D optimization, case 2: only SOC aware 2D optimization, case 3: 1D optimization with fixed SOC and temperature assumption.

slightly skewed to right compared to cases 2 and 3. In case 1, there is a reduction of more than 1 °C in the mean temperature. This is particularly important when we think that this is achieved without active control of the thermal management system (TMS). Then by looking at Figs. 10d–f, we can see SOC distributions in different cases. These figures show that SOC distribution is skewed to right in cases 1–2 whereas it is mostly a uniform distribution in Fig. 10f. Therefore, we infer that SOC awareness also has a substantial effect on SOC distribution and it can reduce the mean SOC from 50% to 35-40% level. A cumulative frequency plot for SOC is given in Appendix in Fig. A2 where uniform distribution of SOC in case 1 can be seen clearly whereas cases 2 and 3 exhibit a similar pattern.

After analyzing the effects of different strategies on the important system variables P_{AC}, SOC and T, we can observe long-term benefits of these strategies by taking a closer look at Fig. 11 and Table 1. In Fig. 11, we see the the actual SOC during the one-year simulation (solid line) and the fitted and extrapolated SOH projection until the end of life (dashed line). We extrapolate the aging behavior through square-root-function defined curve as given in (46), as the function applies well to the mostly square-root-based degradation model in [12]. This equation fits to the aging data with ∼99.9% goodness (according to the adjusted R-squared metric given in Table 1).

$$SOH(t) = 100 - a_{\text{ext}}\sqrt{t} \tag{46}$$

By looking at the three curves in Fig. 11, we see that with each additional level of complexity introduced, battery health is improved considerably. By continuing the degradation trend in the first year, we reach end-of-life times of 7.5, 6.2, 5.3 years for cases 1–3 respectively. This reveals a ∼41% increase in battery life when proposed case (case 1) and the base case (case 3) is compared. In this increase, SOC awareness has a contribution of ∼16% (from 5.3 years to 6.2 years) whereas the additional temperature awareness

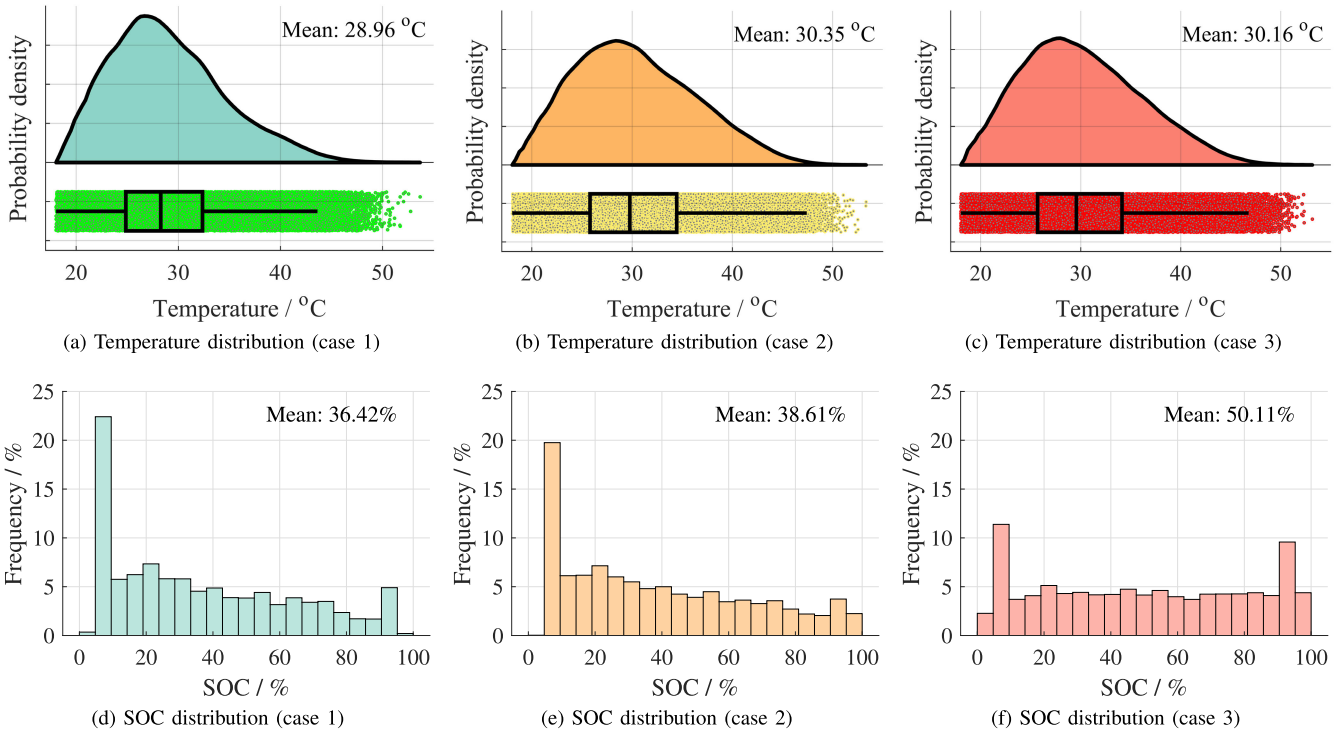

FIGURE 10. Temperature distributions and SOC distributions, where figures (a), (b) and (c) show the raincloud plot of the temperature distribution for cases 1–3 respectively, figures (d), (e) and (f) show the histogram plot of the SOC distribution for cases 1–3 respectively. Case 1: temperature and SOC aware 3D optimization, case 2: only SOC aware 2D optimization, case 3: 1D optimization with fixed SOC and temperature assumption.

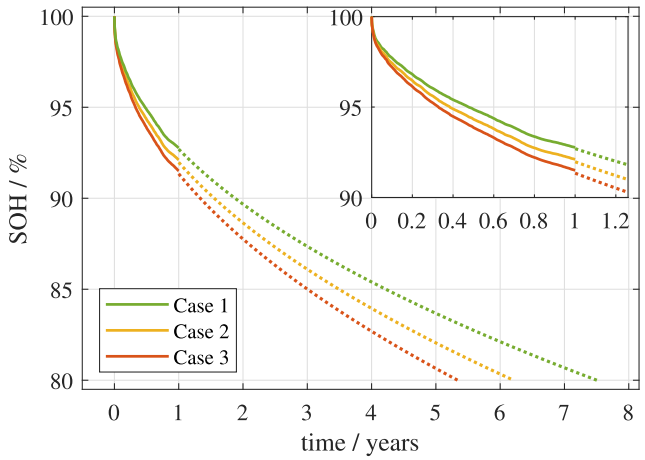

FIGURE 11. SOH evaluation and projection due to temperature and SOC inclusion. Case 1: temperature and SOC aware 3D optimization, case 2: only SOC aware 2D optimization, case 3: 1D optimization with fixed SOC and temperature assumption.

TABLE 1. Estimated parameters for lifetime projection.

	Case 1	Case 2	Case 3
Expected life time (years)	7.5	6.2	5.3
Present value of total revenue (EUR)	92167	81824	73625
Profitability index	**1.92**	**1.70**	**1.53**
Goodness of fitting (%)	99.88	99.88	99.89
a_{ext} (%/$\sqrt{\text{years}}$)	7.30	8.03	8.66

(being a main contribution of this work) has a contribution of ∼21% (from 6.2 years to 7.5 years). As given in Table 1, this increase in battery life may result in a profit increase of ∼25% when case 1 and the base case are compared using a depreciation calculation further explained in the text below. Here, SOC awareness is responsible for an increase of ∼11% (from profitability index 1.53 to 1.70) whereas temperature awareness causes a ∼13% increase (from profitability index 1.70 to 1.92).

To calculate present value of total revenue considering the battery life, we first found mean SOH values for each year with the help of the extrapolation given in Fig. 11. Then, by using the one-year revenue values in Table 2 and mean SOH values for each year, we find the revenue value for each year proportional to the that year's mean SOH value and length of the year. Then a net present value formula is used to find the present value of the revenue. Afterwards, profitability index found by dividing the net present revenue by cost of battery. This process is given by (47)–(50).

$$\mathbb{R}_p = \frac{\overline{SOH}_p}{\overline{SOH}_1}\mathbb{R}_1 \tag{47}$$

$$\mathbb{Y}_p = \{p \text{ if } p \leq \lfloor t_{\text{EOL}} \rfloor \text{ else } t_{\text{EOL}}\} \tag{48}$$

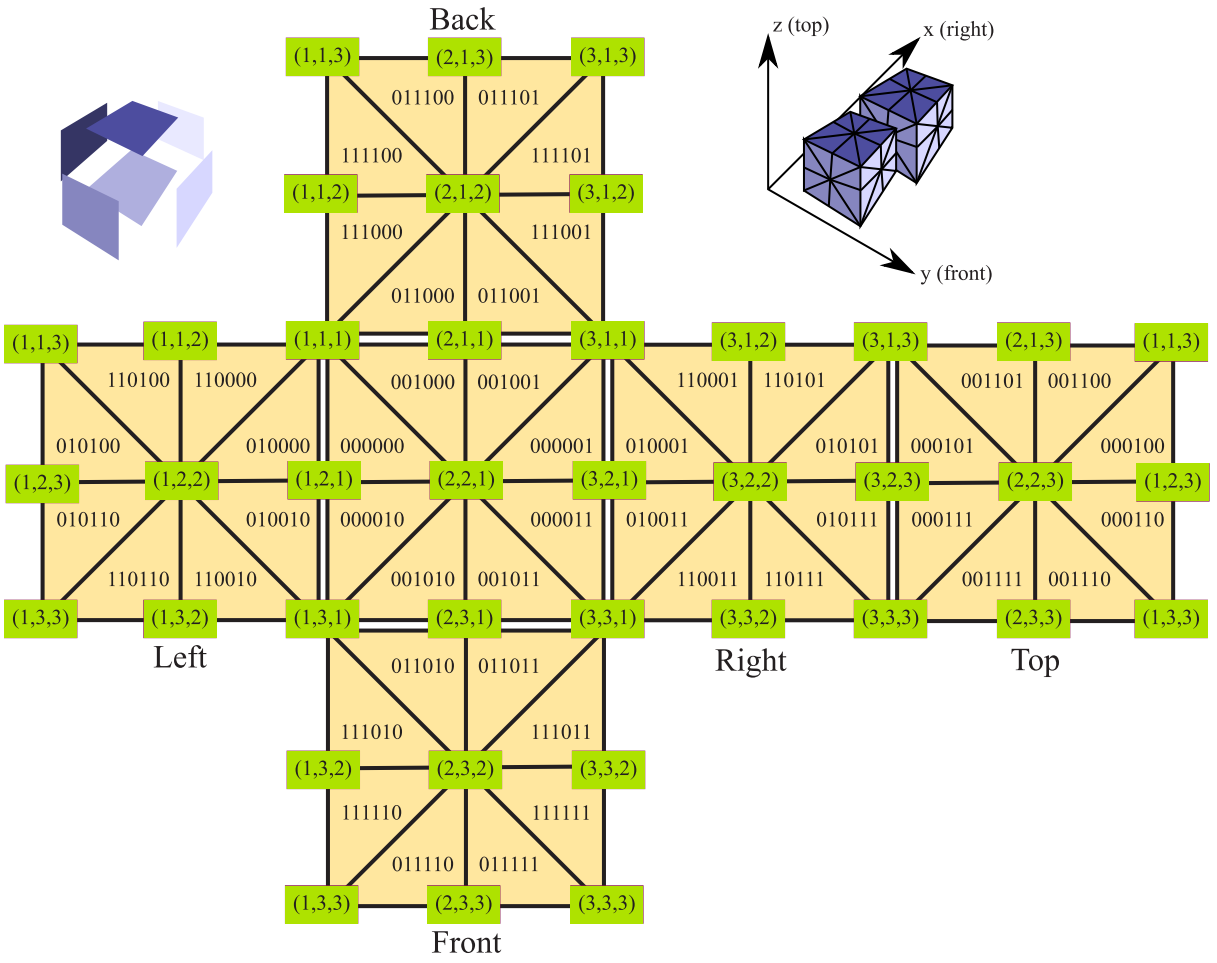

FIGURE A1. Pyramids inside one rectangular prism with their respective gray codes.

$$\mathbb{R}^{\mathrm{PV}} = \sum_{p=1}^{\lceil t_{\mathrm{EOL}} \rceil} \left(\frac{\mathbb{R}_p \cdot (\mathbb{Y}_p - \mathbb{Y}_{p-1})}{(1+i)^{\mathbb{Y}_p}} \right) \tag{49}$$

$$\mathrm{PI} = \mathbb{R}^{\mathrm{PV}} / \mathbb{C}^{\mathrm{investment}} \tag{50}$$

where $\overline{SOH}_p$, $\mathbb{R}_p$, $\mathbb{Y}_p$, t_{EOL}, i, $\mathbb{R}^{\mathrm{PV}}$, PI, $\mathbb{C}^{\mathrm{battery}}$ denote mean SOH for the year p, discounted revenue of year p, year value of the year p, battery end-of-life time in years, interest rate (or cost of capital), total present value of the revenue, profitability index, cost of investment. In this study, cost of capital is taken as $i = 6\%$ and investment cost $\mathbb{C}^{\mathrm{investment}}$ is equal to battery cost $\mathbb{C}^{\mathrm{battery}} = E_{\mathrm{nom}} \cdot c_{\mathrm{bat}}$.

Lastly, the results regarding to one-year simulation are summarized in Table 2. To highlight the importance of the temperature awareness, we have compared effect of temperature and SOC awareness to the inclusion of the power electronics efficiency by considering the study showing the importance of the dynamic power electronics efficiency in [7]. Therefore, cases 1–3 are conducted by neglecting the power electronics efficiency (i.e., changing (7) as $P_{\mathrm{AC}} = P_{\mathrm{b}}$) and named as cases 4–6 respectively. We should also note that when we ignore power electronics efficiency, we ignore it in both optimization and BESS simulation whereas when we exclude the temperature and SOC effects, we exclude them only in the optimization.

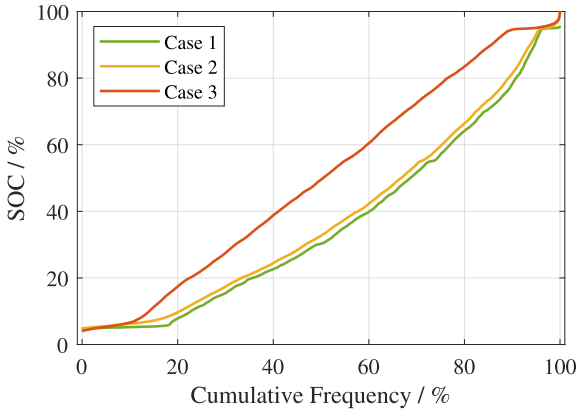

FIGURE A2. *SOC* differences due to temperature and SOC inclusion. Case 1: temperature and SOC aware 3D optimization, case 2: only SOC aware 2D optimization, case 3: 1D optimization with fixed SOC and temperature assumption.

Considering Table 2, the temperature awareness cause more than ∼10% decrease in number of cycles whether power electronics efficiency is included or not. On the other hand,

TABLE 2. System characteristics regarding one-year simulation of the temperature dynamics study considering a 192 kWh_{cap} of battery storage.

Application and Dataset	System characteristics under different included effects					
	Battery and PE losses			Only battery losses		
Are SOC and temperature effects included?	Both	Only SOC	None	Both	Only SOC	None
Case no:	**Case 1**	**Case 2**	**Case 3**	**Case 4**	**Case 5**	**Case 6**
Charge throughput [Ah]	11776	13278	13018	12826	14594	14205
Full equivalent cycle [-]	2062	2337	2301	2249	2573	2515
Mean Temperature [°C]	28.96	30.35	30.16	29.58	31.20	30.98
Mean SOC [%]	36.4	38.6	50.1	36.4	39.4	50.5
SOH [%]	92.77	92.11	91.50	92.62	91.87	91.29
Calendar aging [%]	3.75	4.14	4.82	3.80	4.26	4.92
Cycle aging [%]	3.48	3.75	3.68	3.58	3.87	3.79
Total battery degradation [%]	**7.23**	**7.89**	**8.50**	**7.38**	**8.13**	**8.71**
PE efficiency losses [EUR/year]	922	1018	1010	0	0	0
Battery efficiency losses [EUR/year]	2133	2305	2274	2250	2464	2427
Revenue (after efficiency losses) [EUR/year]	17012	17555	17862	18210	18880	19137
Approximated battery aging losses [EUR/year]	4670	5771	6716	4980	6296	7231
Net profit [EUR/year]	**12342**	**11784**	**11145**	**13229**	**12584**	**11907**

TABLE A1. Optimization parameters.

Parameter	Value	Unit
c_{bat}	250	EUR/kWh_{cap}
k_{EOL}	0.8	–
E_{nom}	192	kWh_{cap}
C_{nom}	3	Ah
SOC_{min}, SOC_{max}	0.05, 0.95	–
T_h, T_a	8, 4	h
T_{sim}	365	days
Δt, δt	1/4, 1/32	h
C^{+}_{rmax}, C^{-}_{rmax}	1, 2	1/h
P^{max}_{AC}	345.6	kW
T_{min}, T_{max}	18, 55	°C
$T_{constant}$	25	°C
$SOC_{constant}$	50%	–
N_{Pcell}, N_{SOC}, N_T	8, 4, 4	–
TimeLimit (worst case)	1500	s
MIP gap	1.8%	–
Cuts	1	–
Presolve	2	–

taking power electronics efficiency into account only causes ∼9% decrease in number of cycles. Hence, we may infer that temperature awareness has a comparable effect on battery usage if not higher than considering power electronics efficiency.

By looking at the aging values, there is a noticeable amount of increase in the battery health. In detail, when SOC and temperature effects are neglected, calendar aging becomes more pronounced. Moreover, temperature awareness cause a reduction in both calendar and cycle aging whereas SOC awareness cause reduction in only calendar aging. In fact, SOC awareness lead to a slight increase in cycle aging, probably due to the faster discharging or more frequent charging and discharging to keep SOC at lower levels.

Net profit values are slightly increased due to the decrease in battery degradation losses despite of not hedging for some of the profit potential of the market signals. It should be noted that battery degradation costs in Table 2 are approximated leveraging (18). Otherwise, direct usage of battery capacity loss would cause overestimation of the battery costs due to the square-root-like shape of the SOH values. Therefore, profit calculations in Table 1 and 2 may differ.

Algorithm A1 Creating Gray Code for Three Dimensional Space

function $grayCode = \text{grayEnum}(n_x, n_y, n_z)$
$n_x,\ n'_x \leftarrow \max(n_x, 1),\quad n_y,\ n'_y \leftarrow \max(n_y, 1),$
$n_z,\ n'_z \leftarrow \max(n_z, 1)$
$d_x \leftarrow \lceil \log_2(n_x, 1) \rceil,\quad d_y \leftarrow \lceil \log_2(n_y, 1) \rceil,$
$d_z \leftarrow \lceil \log_2(n_z, 1) \rceil$
$d_n \leftarrow d_x + d_y + d_z$
$grayCode \leftarrow$ The fundamental cube in Fig. A1
for $i \in [1, \ldots, d_n]$ **do**
  if $n'_x \geq n'_y$ **then**
    $grayCode \leftarrow \text{grayGen}(grayCode,\ \text{x})$
    $n'_x \leftarrow n'_x/2$
  else
    if $n'_y \geq n'_z$ **then**
      $grayCode \leftarrow \text{grayGen}(grayCode,\ \text{y})$
      $n'_y \leftarrow n'_y/2$
    else
      $grayCode \leftarrow \text{grayGen}(grayCode,\ \text{z})$
      $n'_z \leftarrow n'_z/2$
return $grayCode(1 : n_x, 1 : n_y, 1 : n_z)$
end

V. CONCLUSION AND OUTLOOK

In this article, an optimization framework including the thermal dynamics of a battery container is provided. With the help of state of art algorithms leveraging binary counting, a three-dimensional aging model (being dependent on cell power, SOC, and temperature) is embedded into the optimization problem. Then the proposed method is tested for energy intraday market arbitrage operations considering

Algorithm A2 Auxiliary Function to Expand Gray Code Array

1: **function** $grayCode' = \text{grayGen}(grayCode, direction)$
2: // See study [50] for detailed information.
3: // *direction* is the axis to be expanded.
4: $grayCode_0 \leftarrow grayCode$
5: $grayCode_1 \leftarrow$ reflection of $grayCode$ along the plane constructed by two axes other than the *direction* axis.
6: Add new bit 0 to end of bits in all gray codes in $grayCode_0$
7: Add new bit 1 to end of bits in all gray codes in $grayCode_1$
8: $grayCode' \leftarrow$ Concatenation of $grayCode_0$ and $grayCode_1$ along the *direction* axis
9: **return** $grayCode'$
10: **end**

three different levels of model fidelity; three-dimensional aging model, two dimensional aging model (SOC and cell power), and one dimensional aging model (only cell power). On top of that, the effect of increasing model fidelity is compared against the effect of neglecting power electronics efficiency. Lastly, an economic analysis of the profitability of the proposed method is conducted by the extrapolating aging curve.

Results show that modeling thermal dynamics in optimization cause an effect comparable to the impact of power electronic equipment efficiency. Even without active control of the thermal management system, the proposed method reduces cell temperature more than 1 °C. Hence, it raises the expected battery life significantly. As compared to the base case where the expected life was 5.3 years, the proposed method increased battery life by 2.2 years (or 40%) of which 1.3 years is due to the temperature awareness and 0.9 years due to the SOC awareness. This increase in battery lifetime reflects on the revenue as an additional 18.5 thousand EUR compared to the base case. Temperature awareness is responsible for 10.3 thousand EUR of this profit on its own. Considering the battery price of 48 thousand EUR, this increase corresponds to 38.6% of the battery price. In other words, it is additional revenue of more than 25% overall.

Along with its contributions, this study also suffers from several limitations that will be addressed in future studies. The main limitations of this study are given below with their respective future work.

- The price signal information is assumed to be perfect. However, in the real-world, algorithms taking the uncertainty into account should be used [64], [65].
- Thermal dynamics are simplified to a 0-D model. However, with the help of data-driven methods, it would be possible to take the thermal flow in the BESS container into account without relying on computationally intensive computational fluid dynamics simulations [66].
- Active control of the thermal management system is not considered. By leveraging this additional degree of freedom, it may be possible to find an operation strategy reducing cooling costs with a small compromise in battery degradation. On top of that, cooling costs and optimizer decisions can be analyzed under extreme climate conditions of different regions such as Singapore or Norway.
- To keep overall simulation time at reasonable levels, the control horizon is selected as 4 hours. However, a smaller horizon would be needed to make the system more realistic and more resilient against price changes.
- Although only the arbitrage scenario in intraday markets is considered in this study, there are multiple ways of utilizing the BESS. It is possible to reach the maximum potential of BESS by considering the combined operation of multi-use scenarios [67]. Additionally, BESS performance can be improved by hybridizing BESS with other storage systems such as supercapacitors [68].

APPENDIX

Please see Figs. A1 and A2, and Algorithm A1 and Algorithm A2. Fig. A1 shows bases of six square pyramids which form the cube (cf. [69] for unfolded paper version). Each base is located on one face of the cube. Then the bases are triangulated via union-jack triangulation so that they form smaller pyramids with four vertices, three located on the base and one on the top of the pyramid. Gray code of each triangle on the base represents the gray code of each unique small pyramid. Although this type of triangulation looks to have more pyramids compared to R- or K-triangulation, it creates two segments at each axis. If we consider a cuboid with two segments at each axis with a R- or K-triangulation, it would have $2^3 \cdot 6 = 48$ pyramids, same as union jack triangulation.

ACKNOWLEDGEMENTS

Authors would like to thank *Enes Faruk Ballı*, *Başaran Bahadır Koçer*, *Emeç Erçelik* and *Barış Burak Kanbur* for their invaluable discussions and support.

REFERENCES

[1] Á. Arcos-Vargas, D. Canca, and F. Núñez, "Impact of battery technological progress on electricity arbitrage: An application to the iberian market," *Appl. Energy*, vol. 260, Feb. 2020, Art. no. 114273.
[2] P. Fortenbacher, "On the integration of distributed battery storage in low voltage grids," Ph.D. dissertation, ETH Zurich, Zürich, Switzerland, 2017.
[3] A. Hoke, A. Brissette, K. Smith, A. Pratt, and D. Maksimovic, "Accounting for lithium-ion battery degradation in electric vehicle charging optimization," *IEEE J. Emerg. Sel. Topics Power Electron.*, vol. 2, no. 3, pp. 691–700, Sep. 2014.
[4] G. Wang, G. Konstantinou, C. D. Townsend, J. Pou, S. Vazquez, G. D. Demetriades, and V. G. Agelidis, "A review of power electronics for grid connection of utility-scale battery energy storage systems," *IEEE Trans. Sustain. Energy*, vol. 7, no. 4, pp. 1778–1790, Oct. 2016.
[5] M. Schimpe, C. Piesch, H. Hesse, J. Paß, S. Ritter, and A. Jossen, "Power flow distribution strategy for improved power electronics energy efficiency in battery storage systems: Development and implementation in a utility-scale system," *Energies*, vol. 11, no. 3, p. 533, Mar. 2018.
[6] M. Schimpe, "System simulation of utility-scale lithium-ion battery energy storage systems," Ph.D. dissertation, Technische Universität München, München, Germany, 2019.

[7] H. Hesse, V. Kumtepeli, M. Schimpe, J. Reniers, D. Howey, A. Tripathi, Y. Wang, and A. Jossen, "Ageing and efficiency aware battery dispatch for arbitrage markets using mixed integer linear programming," *Energies*, vol. 12, no. 6, p. 999, Mar. 2019.

[8] B. Xu, J. Zhao, T. Zheng, E. Litvinov, and D. S. Kirschen, "Factoring the cycle aging cost of batteries participating in electricity markets," *IEEE Trans. Power Syst.*, vol. 33, no. 2, pp. 2248–2259, Mar. 2018.

[9] M. Seydenschwanz, K. Majewski, C. Gottschalk, and R. Fink, "Linear approximation of cyclic battery aging costs for MILP-based power dispatch optimization," in *Proc. IEEE PES Innov. Smart Grid Technol. Eur. (ISGT-Eur.)*, Sep. 2019, pp. 1–5.

[10] M. Schimpe, M. Naumann, N. Truong, H. C. Hesse, S. Santhanagopalan, A. Saxon, and A. Jossen, "Energy efficiency evaluation of a stationary lithium-ion battery container storage system via electro-thermal modeling and detailed component analysis," *Appl. Energy*, vol. 210, pp. 211–229, Jan. 2018.

[11] J. Vetter *et el.*, "Ageing mechanisms in lithium-ion batteries," *J. Power Sources*, vol. 147, nos. 1–2, pp. 269–281, 2005.

[12] M. Schimpe, M. E. von Kuepach, M. Naumann, H. C. Hesse, K. Smith, and A. Jossen, "Comprehensive modeling of temperature-dependent degradation mechanisms in lithium iron phosphate batteries," *J. Electrochemical Soc.*, vol. 165, no. 2, pp. A181–A193, 2018.

[13] V. Kumtepeli, Y. Zhao, M. Naumann, A. Tripathi, Y. Wang, A. Jossen, and H. C. Hesse, "Design and analysis of an aging-aware energy management system for islanded grids using mixed-integer quadratic programming," *Int. J. Energy Res.*, vol. 43, no. 9, pp. 4127–4147, 2019.

[14] M. Naumann, F. B. Spingler, and A. Jossen, "Analysis and modeling of cycle aging of a commercial LiFePO4/graphite cell," *J. Power Sources*, vol. 451, Mar. 2020, Art. no. 227666.

[15] C. Goebel, H. Hesse, M. Schimpe, A. Jossen, and H.-A. Jacobsen, "Model-based dispatch strategies for lithium-ion battery energy storage applied to pay-as-bid markets for secondary reserve," *IEEE Trans. Power Syst.*, vol. 32, no. 4, pp. 2724–2734, Jul. 2017.

[16] M. Naumann, C. N. Truong, M. Schimpe, D. Kucevic, A. Jossen, and H. C. Hesse, "Simses: Software for techno-economic simulation of stationary energy storage systems," in *Proc. Int. ETG Congr.*, 2017, pp. 1–6.

[17] A. Ulbig, T. S. Borsche, and G. Andersson, "Analyzing rotational inertia, grid topology and their role for power system stability," *IFAC-PapersOnLine*, vol. 48, no. 30, pp. 541–547, 2015.

[18] M. McPherson and S. Tahseen, "Deploying storage assets to facilitate variable renewable energy integration: The impacts of grid flexibility, renewable penetration, and market structure," *Energy*, vol. 145, pp. 856–870, Feb. 2018. [Online]. Available: [Online]. Available: http://www.sciencedirect.com/science/article/pii/S0360544218300021

[19] T. Weitzel and C. H. Glock, "Energy management for stationary electric energy storage systems: A systematic literature review," *Eur. J. Oper. Res.*, vol. 264, no. 2, pp. 582–606, Jan. 2018. [Online]. Available: [Online]. Available: http://www.sciencedirect.com/science/article/pii/S0377221717305933

[20] M. Schimpe, C. N. Truong, M. Naumann, A. Jossen, H. C. Hesse, J. M. Reniers, and D. A. Howey, "Marginal costs of battery system operation in energy arbitrage based on energy losses and cell degradation," in *Proc. IEEE Int. Conf. Environ. Electr. Eng. IEEE Ind. Commercial Power Syst. Eur. (EEEIC/ICPS Europe)*, Piscataway, NJ, USA, Jun. 2018, pp. 1–5.

[21] J. M. Reniers, G. Mulder, S. Ober-Blöbaum, and D. A. Howey, "Improving optimal control of grid-connected lithium-ion batteries through more accurate battery and degradation modelling," *J. Power Sour.*, vol. 379, pp. 91–102, Mar. 2018. [Online]. Available: http://www.sciencedirect.com/science/article/pii/S0378775318300041

[22] M. Naumann, M. Schimpe, P. Keil, H. C. Hesse, and A. Jossen, "Analysis and modeling of calendar aging of a commercial LiFePO4/graphite cell," *J. Energy Storage*, vol. 17, pp. 153–169, Jun. 2018.

[23] M. Schimpe, M. E. von Kuepach, M. Naumann, H. C. Hesse, A. Jossen, K. Smith, and S. Santhanagopalan, "Semi-empirical modeling of temperature-dependent degradation mechanisms in lithium-ion batteries," in *Proc. Meeting Abstr.*, vol. MA2017-02, 2017, p. 19.

[24] M. Schimpe, M. E. von Kuepach, M. Naumann, H. C. Hesse, K. Smith, and A. Jossen, "Comprehensive modeling of temperature-dependent degradation mechanisms in lithium iron phosphate batteries," *ECS Trans.*, vol. 80, p. 147, Oct. 2017.

[25] U. Can Yilmaz, M. Erdem Sezgin, and M. Go, "A model predictive control for microgrids considering battery aging," *J. Mod. Power Syst. Clean Energy*, vol. 8, no. 2, pp. 296–304, 2020.

[26] D. Metz and J. T. Saraiva, "Use of battery storage systems for price arbitrage operations in the 15- and 60-min german intraday markets," *Electr. Power Syst. Res.*, vol. 160, pp. 27–36, Jul. 2018. [Online]. Available: http://www.sciencedirect.com/science/article/pii/S0378779618300282

[27] M. Jafari, A. Botterud, and A. Sakti, "Estimating revenues from offshore wind-storage systems: The importance of advanced battery models," *Appl. Energy*, vol. 276, Oct. 2020, Art. no. 115417. [Online]. Available: https://www.sciencedirect.com/science/article/pii/S0306261920309296

[28] A. Sakti, K. G. Gallagher, N. Sepulveda, C. Uckun, C. Vergara, F. J. de Sisternes, D. W. Dees, and A. Botterud, "Enhanced representations of lithium-ion batteries in power systems models and their effect on the valuation of energy arbitrage applications," *J. Power Sources*, vol. 342, pp. 279–291, Feb. 2017.

[29] R. Misener and C. A. Floudas, "Piecewise-linear approximations of multidimensional functions," *J. Optim. Theory Appl.*, vol. 145, no. 1, pp. 120–147, Apr. 2010.

[30] J. P. Vielma, S. Ahmed, and G. Nemhauser, "Mixed-integer models for nonseparable piecewise-linear optimization: Unifying framework and extensions," *Oper. Res.*, vol. 58, no. 2, pp. 303–315, Apr. 2010.

[31] J. P. Vielma, "Embedding formulations and complexity for unions of polyhedra," *Manage. Sci.*, vol. 64, no. 10, pp. 4721–4734, Oct. 2018.

[32] G. L. Plett, *Battery Management Systems: Battery Modeling*, vol. 1. Norwood, MA, USA: Artech House, 2015.

[33] K. Rumpf, M. Naumann, and A. Jossen, "Experimental investigation of parametric cell-to-cell variation and correlation based on 1100 commercial lithium-ion cells," *J. Energy Storage*, vol. 14, pp. 224–243, Dec. 2017. [Online]. Available: http://www.sciencedirect.com/science/article/pii/S2352152X17302633

[34] K. E. Thomas and J. Newman, "Thermal modeling of porous insertion electrodes," *J. Electrochem. Soc.*, vol. 150, no. 2, p. A176, 2003.

[35] J. Shim and K. A. Striebel, "Cycling performance of low-cost lithium ion batteries with natural graphite and LiFePO4," *J. Power Sources*, vols. 119–121, pp. 955–958, Jun. 2003. [Online]. Available: http://www.sciencedirect.com/science/article/pii/S0378775303002970

[36] G. L. Plett, *Battery Management Systems: Equivalent-circuit Methods*, vol. 2. Norwood, MA, USA: Artech House, 2015.

[37] R. Martins, H. Hesse, J. Jungbauer, T. Vorbuchner, and P. Musilek, "Optimal component sizing for peak shaving in battery energy storage system for industrial applications," *Energies*, vol. 11, no. 8, p. 2048, Aug. 2018.

[38] E. V. Thomas, I. Bloom, J. P. Christophersen, and V. S. Battaglia, "Rate-based degradation modeling of lithium-ion cells," *J. Power Sources*, vol. 206, pp. 378–382, May 2012.

[39] E. V. Thomas, I. Bloom, J. P. Christophersen, D. C. Robertson, L. K. Walker, C. D. Ho, and V. S. Battaglia, "Modeling memoryless degradation under variable stress," *J. Qual. Technol.*, vol. 51, no. 3, pp. 284–299, Jul. 2019.

[40] J. Schmalstieg, S. Käbitz, M. Ecker, and D. U. Sauer, "A holistic aging model for Li(NiMnCo)O2 based 18650 lithium-ion batteries," *J. Power Sour.*, vol. 257, pp. 325–334, Jul. 2014.

[41] F. M. Gatta, A. Geri, S. Lauria, M. Maccioni, and F. Palone, "Battery energy storage efficiency calculation including auxiliary losses: Technology comparison and operating strategies," in *Proc. IEEE Eindhoven PowerTech*, Jun. 2015, pp. 1–6.

[42] M. Naumann, C. N. Truong, M. Schimpe, D. Kucevic, A. Jossen, and H. C. Hesse, "Simses: Software for techno-economic simulation of stationary energy storage systems," in *Proc. Int. ETG Congr.*, 2017, pp. 1–6.

[43] M. Schimpe, N. Becker, T. Lahlou, H. C. Hesse, H.-G. Herzog, and A. Jossen, "Energy efficiency evaluation of grid connection scenarios for stationary battery energy storage systems," *Energy Procedia*, vol. 155, pp. 77–101, Nov. 2018.

[44] E. M. L. Beale and J. J. H. Forrest, "Global optimization using special ordered sets," *Math. Program.*, vol. 10, no. 1, pp. 52–69, Dec. 1976.

[45] R. Misener, C. E. Gounaris, and C. A. Floudas, "Global optimization of gas lifting operations: A comparative study of piecewise linear formulations," *Ind. Eng. Chem. Res.*, vol. 48, no. 13, pp. 6098–6104, Jul. 2009.

[46] J. Huchette and J. Pablo Vielma, "Nonconvex piecewise linear functions: Advanced formulations and simple modeling tools," 2017, *arXiv:1708.00050*. [Online]. Available: http://arxiv.org/abs/1708.00050

[47] J. A. Huchette, "Advanced mixed-integer programming formulations: Methodology, computation, and application," Ph.D. dissertation, Massachusetts Inst. Technol., Cambridge, MA, USA, 2018.

[48] D. J. Malan, "Reinventing CS50," in *Proc. 41st ACM Tech. Symp. Comput. Sci. Educ.*, 2010, pp. 152–156.
[49] E. Kalvelagen. (Jul. 2019). *Piecewise Linear Functions and Formulations for Interpolation (Part 3)*. [Online]. Available: https://yetanothermathprogrammingconsultant.blogspot.com/2019/03/piecewise-linear-functions-and.html
[50] T. Strang, A. Dammann, M. Roeckl, and S. Plass, "Using gray codes as location identifiers," Geographisches Institut, Univ. Heidelberg, Heidelberg, Germany, Tech. Rep., 2009, vol. 1, pp. 135–143. [Online]. Available: https://www.semanticscholar.org/paper/Using-Gray-codes-as-Location-Identifiers-Strang-Dammann/1eb1acd04eaa9475-afc173666ccacc1651-a6532c
[51] J. Huchette, S. S. Dey, and J. P. Vielma, "Strong mixed-integer formulations for the floor layout problem," *INFOR, Inf. Syst. Oper. Res.*, vol. 56, no. 4, pp. 392–433, Oct. 2018.
[52] S. van der Walt, S. C. Colbert, and G. Varoquaux, "The NumPy array: A structure for efficient numerical computation," *Comput. Sci. Eng.*, vol. 13, no. 2, pp. 22–30, Mar. 2011.
[53] P. Luathep, A. Sumalee, W. H. K. Lam, Z.-C. Li, and H. K. Lo, "Global optimization method for mixed transportation network design problem: A mixed-integer linear programming approach," *Transp. Res. B, Methodol.*, vol. 45, no. 5, pp. 808–827, Jun. 2011.
[54] M. Kvasnica, A. Szúcs, and M. Fikar, "Automatic derivation of optimal piecewise affine approximations of nonlinear systems," *IFAC Proc. Vols.*, vol. 44, no. 1, pp. 8675–8680, Jan. 2011.
[55] J. Stevek, A. Szucs, M. Kvasnica, S. Kozak, and M. Fikar, "Smart technique for identifying hybrid systems," in *Proc. IEEE 10th Int. Symp. Appl. Mach. Intell. Informat. (SAMI)*, Jan. 2012, pp. 383–388.
[56] A. Szúcs, M. Kvasnica, and M. Fikar, "Optimal piecewise affine approximations of nonlinear functions obtained from measurements," *IFAC Proc. Volumes*, vol. 45, no. 9, pp. 160–165, 2012.
[57] V. Kumtepeli, Y. Wang, and A. Tripathi, "Multi-area model predictive load frequency control: A decentralized approach," in *Proc. Asian Conf. Energy, Power Transp. Electrific. (ACEPT)*, Piscataway, NJ, USA, Oct. 2016, pp. 1–5.
[58] J. Lofberg, "YALMIP: A toolbox for modeling and optimization in MATLAB," in *Proc. IEEE Int. Conf. Robot. Autom.*, Taipei, Taiwan, 2004, pp. 284–289.
[59] Gurobi Optimization Inc. (2016). *Gurobi Optimizer Reference Manual*. Accessed: Oct. 19, 2018. [Online]. Available: http://www.gurobi.com
[60] E. Spot. (Jan. 21, 2020). *Epex Intraday Market Data*. [Online]. Available: https://www.epexspot.com/de/marktdaten/
[61] M. Allen, D. Poggiali, K. Whitaker, T. R. Marshall, and R. Kievit. (2018). *RainCloudPlots Tutorials and Codebase (Version v1.1)*. Zenodo. [Online]. Available: https://github.com/RainCloudPlots/RainCloudPlots, doi: 10.5281/zenodo.3368186.
[62] M. Allen, D. Poggiali, K. Whitaker, T. R. Marshall, and R. A. Kievit, "Raincloud plots: A multi-platform tool for robust data visualization," *Wellcome Open Res.*, vol. 4, p. 63, Apr. 2019.
[63] Charles. *Cbrewer: Colorbrewer Schemes for MATLAB*. Accessed: Feb. 10, 2020. [Online]. Available: https://www.mathworks.com/matlabcentral/fileexchange/34087-cbrewer-colorbrewer-schemes-for-matlab
[64] Ç. Iris and J. S. L. Lam, "Recoverable robustness in weekly berth and quay crane planning," *Transp. Res. B, Methodol.*, vol. 122, pp. 365–389, Apr. 2019.
[65] Ç. Iris and J. S. L. Lam, "A review of energy efficiency in ports: Operational strategies, technologies and energy management systems," *Renew. Sustain. Energy Rev.*, vol. 112, pp. 170–182, Sep. 2019.
[66] B. B. Kanbur, V. Kumtepeli, and F. Duan, "Thermal performance prediction of the battery surface via dynamic mode decomposition," *Energy*, vol. 201, Jun. 2020, Art. no. 117642. [Online]. Available: http://www.sciencedirect.com/science/article/pii/S0360544220307490c
[67] S. Englberger, H. Hesse, N. Hanselmann, and A. Jossen, "SimSES multi-use: A simulation tool for multiple storage system applications," in *Proc. 16th Int. Conf. Eur. Energy Market (EEM)*, Sep. 2019, pp. 1–5.
[68] S. D. V. R. Vadlamudi, V. Kumtepeli, S. Ozcira, and A. Tripathi, "Hybrid energy storage power allocation and motor control for electric forklifts," in *Proc. Asian Conf. Energy, Power Transp. Electrific. (ACEPT)*, Piscataway, NJ, USA, Oct. 2016, pp. 1–5.
[69] G. K. Altes. *Paper Six Pyramids That Form a Cube*. Accessed: Feb. 4, 2020. [Online]. Available: https://www.polyhedra.net/en/model.php?name-en=six-pyramids-that-form-a-cube

VOLKAN KUMTEPELI received the B.Sc. degree from Yıldız Technical University, Istanbul, Turkey, in 2015, and the Ph.D. degree from the Energy Research Institute, Nanyang Technological University, Singapore, in 2020. His current research interests include grid-scale energy storage systems, power electronics, data-driven, and safe learning approaches and their intersection with model-based optimization methods.

HOLGER C. HESSE received the M.Sc. (diploma) and Ph.D. degrees in physics from the University of Munich, Germany, in 2008 and 2011, respectively. He was a Development Engineer of electric mobility with Bertrandt AG. Since 2014, he has been with the Technical University of Munich, working as a Principal Investigator and a Assistant Head with the Institute for Electrical Energy Storage Technology. His research team analyzes the techno-economic feasibility of stationary battery storage systems in power grids via experimental tests, modeling, and optimization techniques.

MICHAEL SCHIMPE received the M.Sc. degree in mechanical engineering from the Technical University of Munich (TUM), Germany, after studies at TUM and at Nanyang Technological University, Singapore, and the Ph.D. degree in electrical engineering from the Technical University of Munich, in 2019. He conducted his research at the Institute for Electrical Energy Storage Technology, TUM, also at the University of Oxford, U.K., also at Imperial College London, U.K., and also at the National Renewable Energy Laboratory, Department of Energy, USA. His research interests include lithium-ion battery systems and their energy efficiency and battery lifetime.

ANSHUMAN TRIPATHI received the M.Tech. degree from IIT Kanpur, in 1999, and the Ph.D. degree from the National University of Singapore, in 2004.

He has been a Program Director with the Energy Research Institute @ NTU (ERI@N), since November 2012. As the Head of Future Mobility Systems, he has spent last five years in developing autonomous and electric vehicle platforms for public transport and industrial applications, with his multidisciplinary group of researchers and engineers. Before joining ERI@N, he has spent many years in the Industry and Academia. At General Electric, he formed electrical machine design competence in GE-global research delivering machine-converter solutions to GE transportation and GE healthcare systems. He also worked on wireless power transfer solutions for GE healthcare and GE-NBC. He then joined Vestas Wind Power Systems, where he was instrumental in forming a 2- and 3-MW converter design group comprising of hardware, software, and control groups. This group delivered solutions for V-90, V-112, and V-164 turbine platforms of Vestas. He has 37 granted patents, over 75 publications and two start-up companies dealing with energy storage systems and autonomous vehicles design solutions. His research interests include grid connection of large and remote wind and solar farms, grid codes and compliance, power hardware in the loop simulations for power network designs, electrical drive train designs for electric vehicles and hybrid energy storage for stationary and mobile applications.

YOUYI WANG (Senior Member, IEEE) received the B.Eng. degree from the University of Science and Technology Beijing, Beijing, China, in 1982, the M.Eng. degree from Tsinghua University, Beijing, in 1984, and the Ph.D. degree from The University of Newcastle, Australia, in 1991, all in electrical engineering. He is currently a Full Professor with the School of Electrical and Electronic Engineering, Nanyang Technological University, Singapore. Since 1991, he has authored or coauthored more than 400 published international journal and conference articles on control, stability analysis, system theory, the control applications of power systems, electric drive systems, information storage systems, and renewable energy systems. He has also been the principal investigator for more than 20 research and industrial projects. His current research interests include nonlinear control, robust control, H_∞ control and applications of control theory to power systems, electric drive systems, information storage systems, and renewable energy systems.

ANDREAS JOSSEN received the Diploma and Ph.D. degrees in electrical engineering from the University of Stuttgart, Germany, in 1989 and 1994, respectively. From 1994 to 2010, he was with the Centre for Solar Energy and Hydrogen Research, Ulm, Germany, where he was a Leader of the Battery System Technology Group. Since 2010, he has been a Full Professor with the Technical University of Munich, Munich, Germany, where he founded and established the Institute for Electrical Energy Storage Technology. His research interests include the modeling, simulation, and characterization of rechargeable batteries, and fundamental and applied topics in battery systems, such as battery topologies, state determination, and the control of battery systems.